A particle undergoing a 1-dimensional random walk has mean position equal to its original position:

$< x_{random} > \ = \ x_0$

Displacement due to drift is given by $v_d t$ (this is a rearrangement of $v_d = \frac{\Delta x}{t}$), hence the total drift velocity:

$x_{drift} = v_d t + x_{random}$

There is no randomness associated with constant drift velocity, so $< v_d t > \ = \ v_d t$. Therefore:

$< x >_{drift} = \ < v_d t + x_{random} > \ = \ < v_d t > \ + \ < x_{random} >$

$< x >_{drift} = \ v_d t \ + \ x_0$

The mean square displacement for just the random walk is given by:

$< (x_{random} - x_0)^2 >= 2Dt$

$< x^2 >_{drift} = \ < (v_d t)^2 > \ + \ 2 < v_d t (x_{random} - x_0) > \ + \ < (x_{random} - x_0)^2 >$

$< x^2 >_{drift} = \ < (v_d t)^2 > \ + \ 2 < v_d t (x_0 - x_0) > \ + \ < (x_{random} - x_0)^2 >$

(Center term becomes 0 due to 0 net displacement)

$< x^2 >_{drift} = \ (v_d t)^2 \ + \ 2Dt$

Figure 1: Mean square displacement (μm^2) vs. time (s) at different velocities (log-log graph)

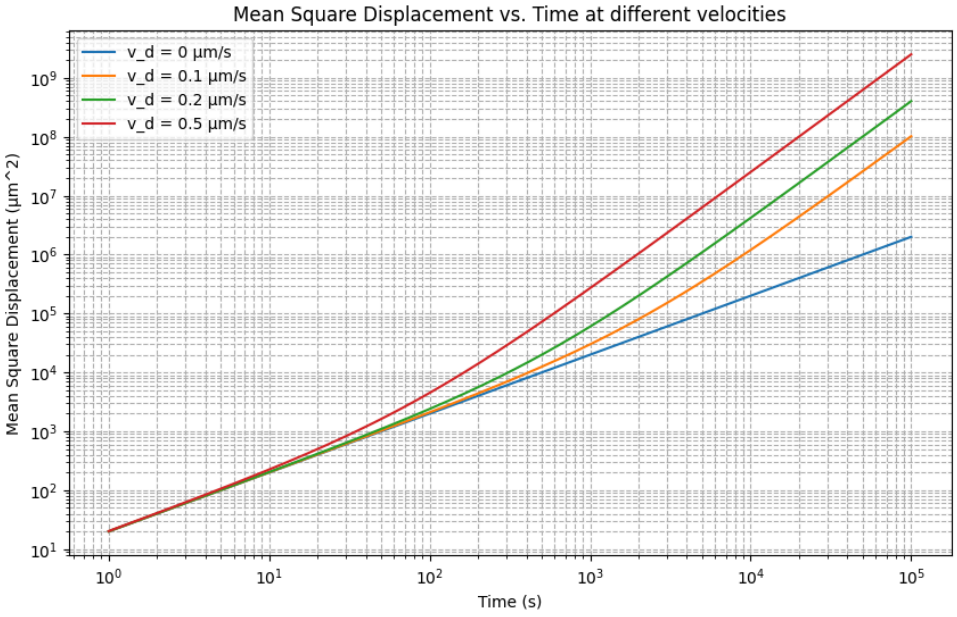

The slope was calculated using Python, by selecting two time values, calculating the mean square displacement at both, and taking the log of both the time and mean square displacements, then dividing the change in log of the mean square displacement over the log of the change in time. The slope with diffusion-dominated motion is around 1. The slope with velocity-dominated motion is around 2. With velocities that are in-between (ex. at 0.1μm/s), we note that the particle more closely embodies diffusion-dominated motion at lower times and velocity-dominated motion at higher times. This makes sense given that the t in the velocity term grows in a quadratic fashion, compared to the t in the random walk term.

Python

```python
import numpy as np
import matplotlib.pyplot as plt

D = 10 # we set our diffusion coefficient (μ^2 /s)

def mean_square_displacement(t, D, v_d):
    return 2 * D * t + (v_d * t) ** 2

time = np.logspace(0, 5, 100000) # we create time values from 1 to 100000

velocities = [0, 0.1, 0.2, 0.5] # we generate multiple velocity values

plt.figure(figsize=(10,6))
for v in velocities:
    plt.loglog(time, mean_square_displacement(time, D, v), label=f"v_d =
{v} μm/s")

plt.xlabel("Time (s)")
plt.ylabel("Mean Square Displacement (μm^2)")
plt.title("Mean Square Displacement vs. Time at different velocities")
plt.legend()
plt.show()
```

```python
v = 0 # variable velocity

# select two points on the line to calculate slope
id1 = 0
id2 = 100

t1 = time[id1]
t2 = time[id2]

log_msd1 = np.log(mean_square_displacement(t1, D, v))
log_msd2 = np.log(mean_square_displacement(t2, D, v))

log_t1 = np.log(t1)
log_t2 = np.log(t2)

slope = (log_msd2 - log_msd1) / (log_t2 - log_t1)
print(slope)
```

Equation for mean-squared displacement with drift:

$$< x^2>_{drift} = (v_d t)^2 + 2Dt$$

Equation for mean-squared displacement without drift

$$< x^2 > = 2Dt$$

The true size of yeast cells obviously varies, but diploid cells are reported to have an ellipsoid shape with size 5×6 μm , and haploid cells 4 μm spheroids (Sherman, 2002). If we take the length of the cell to be 6 μm:

$$t = \frac{<x^2>}{2D}$$

$$t = \frac{(6\mu m)^2}{2(5\ \mu m^2/s)}$$

$$t = 3.6s$$

Rearranging for when mean-squared displacement includes a constant drift velocity from dynein:

$$< x^2>_{drift} = (v_d t)^2 + 2Dt$$

$$0 = (v_d t)^2 + 2Dt - < x^2>_{drift}$$

$$t = \frac{-2D \pm \sqrt{(2D)^2 - 4(v_d)^2(-(x^2)_{drift})}}{2(v_d)^2}$$

$$t = \frac{-2(5) \pm \sqrt{(2(5))^2 - 4(2)^2(-(6^2))}}{2(2)^2} = \frac{-10 \pm \sqrt{568}}{8}$$

$$t = 1.8s$$

The length of a moving fibroblast is reported to be 100μm (McDougall et al., 2006).

$$t_{no\ drift} = \frac{(100\mu m)^2}{2(5\ \mu m^2/s)} = 200.0s$$

$$t_{drift} = \frac{-2(5) \pm \sqrt{(2(5))^2 - 4(2)^2(-(100^2))}}{2(2)^2} = 48.8s$$

We can easily see that in the equation without drift velocity, the dependence on time is linear. Meanwhile, in the equation with drift velocity, the dependence on time is quadratic. Therefore, as the time term grows, the mean-squared displacement of the particle grows much more quickly if there is additional drift velocity.

The opposite relation is true: if the length is very large, then the time term for displacement with drift will be smaller compared to displacement without drift. The displacement term is linear in the time equation for displacement with drift, and quadratic in the time equation for displacement without drift. We can conclude that over long distances, it is not efficient to rely on just diffusion as a transport method.

References

McDougall, S., Dallon, J., Sherratt, J., & Maini, P. (2006). Fibroblast migration and collagen deposition during dermal wound healing: mathematical modelling and clinical implications. *Philos Trans A Math Phys Eng Sci*, *364*(1843), 1385-1405. doi.org/10.1098/rsta.2006.1773

Sherman, F. (2002). Getting started with yeast. *Methods in Enzymology*, *350*, 3-41. doi.org/10.1016/s0076-6879(02)50954-x

Rearranging the given equation for L_p:

$cos(\theta) = e^{-\frac{s}{2Lp}}$

$L_p = -\frac{s}{2ln(cos(\theta))}$

I created a Python script to manually click on an image and add points along a filament. I modeled the filament using a spline curve to interpolate between these points. I approximated the curve's length by sampling 1,000 points and calculating the Euclidean distance between them. I then found the tangent lines at the endpoints by calculating the first derivative for the slope and used the two lines to determine the angle between the lines. I took care to choose a short segment of the filament that contained just a single curve (with one local maximum and one local minimum). The 10 microtubule filaments were taken from the myoblast, and the 10 actin filaments from the fibroblast. In both images, 100 pixels corresponded to 10000 nm.

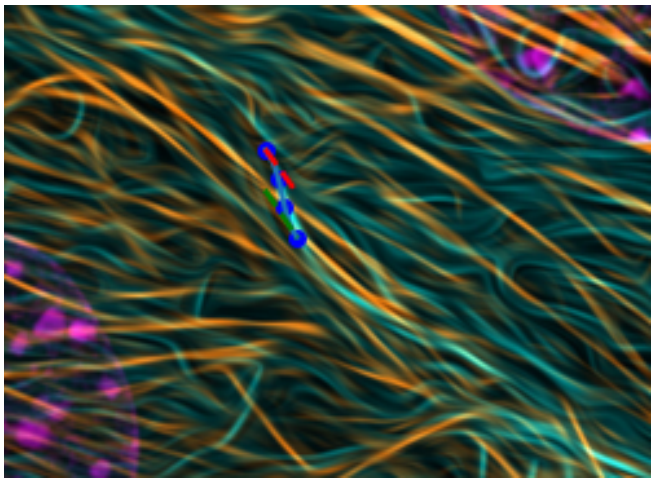

Length of the smooth curve: 112.98501392498876 pixels, 11298.501392498876 nm
Angle in radians: 0.034688958393162425

Sample	Length of curve (μm)	Angle	Persistence length (μm)	Sample	Length of curve (μm)	Angle	Persistence length (μm)
microtubule_1	10.0	0.2	242.6	actin_1	8.2	1.2	4.1
microtubule_2	11.3	0.1	544.9	actin_2	3.1	1.2	1.5
microtubule_3	13.4	0.1	618.9	actin_3	5.0	1.1	3.2
microtubule_4	10.4	0.3	113.2	actin_4	4.4	0.7	8.6
microtubule_5	11.6	0.1	824.8	actin_5	5.5	1.5	1.2
microtubule_6	9.1	0.4	66.9	actin_6	4.9	1.2	2.6
microtubule_7	10.6	0.3	96.1	actin_7	4.1	0.9	4.1
microtubule_8	10.2	0.1	629.8	actin_8	3.5	1.1	2.4
microtubule_9	10.6	0.2	430.4	actin_9	5.5	1.3	2.0
microtubule_10	12.8	0.3	148.5	actin_10	5.1	0.9	5.2

Figure 1: Distribution of persistence lengths of 10 microtubules

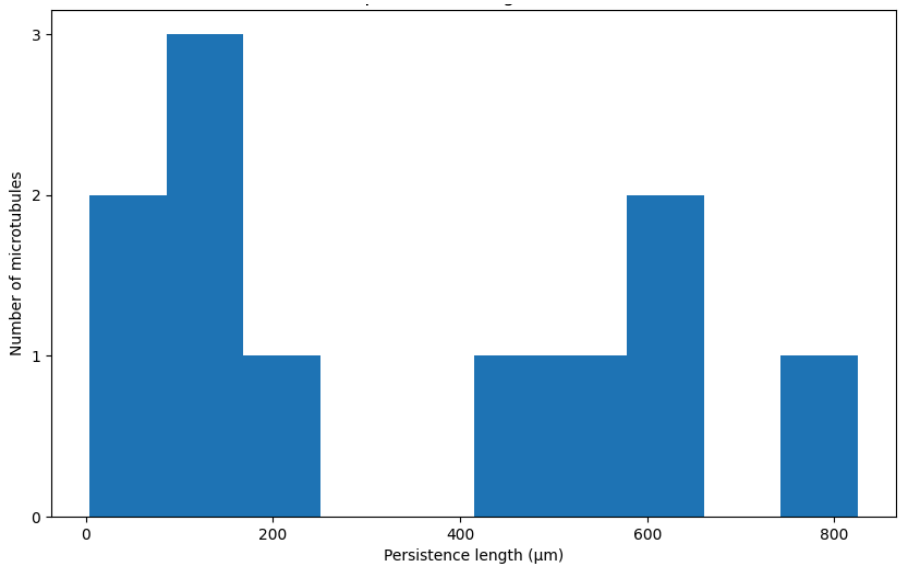

Source	Persistence length of microtubules (μm)
Own procedure	338 (s.t.d 268)
Gittes, F., Mickey, B., Nettleton, J., & Howard, J. (1993).	5200
Wisanpitayakorn, P., Mickolajczyk, K. J., Hancock, W. O., Vidali, L., & Tüzel, E. (2022).	310 ± 90
Niederriter, G., & Martin, D. S. (2019).	Length <3: 0.15 to 4.5 Length 4.5 - 15: 500 to 1800

Figure 2: Distribution of persistence lengths of 10 actin filaments

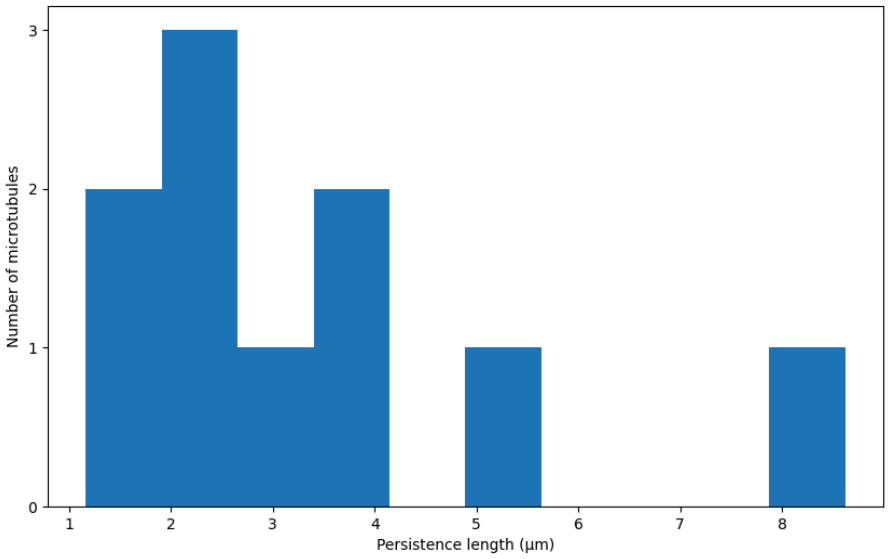

Source	Persistence length of microtubules (μm)
Own procedure	3.5 (s.t.d 2.1)
Gittes, F., Mickey, B., Nettleton, J., & Howard, J. (1993).	17.7
Wisanpitayakorn, P., Mickolajczyk, K. J., Hancock, W. O., Vidali, L., & Tüzel, E. (2022).	9.9 ± 1.1
Isambert, H., Venier, P., Maggs, A. C., Fattoum, A., Kassab, R., Pantaloni, D., & Carlier, M.-F. (1995).	9 - 20

	Microtubule	Actin
Mean (μm)	338	3.5
Standard deviation (μm)	268	2.1

The persistence length for microtubules was found to be within literature values with Wisanpitayakorn et. al, albeit with extreme variation across the 10 samples. However, it deviated significantly from persistence lengths found in other studies. The persistence length for actin filaments was significantly lower than all literature values. Overall, the procedure correctly replicated the pattern of actin filament persistence lengths being several degrees smaller than those of microtubule filaments (around 100 times smaller). The distribution of both actin and microtubule filament lengths fails to follow a normal distribution, most likely because of the small sample size. In addition, Wisanpitayakorn et. al note that the persistence length of filaments depends highly on interactions with nearby filaments or proteins in the cell. Visually, it is clear that certain filaments appear straighter than others, particularly those that cluster into long bundles of filaments. It is possible that interactions with nearby filaments can contribute to apparent stiffness.

The procedure introduces a lot of randomness, particularly since the resolution of the filaments was low compared to the rest of the image. With every point not being placed perfectly along the contour of the filament, the resulting spline curve's accuracy is affected. Since I was picking very short segments (~3-10 μm), I also introduced a greater degree of measurement uncertainty. The procedure could have been improved by picking not the tangent lines at the endpoints (since the slope at the endpoints may not properly represent the rest of the curve) but rather somewhere in the middle of the curve. Taking more than 10 samples would also aid in reducing sampling error and random errors.

The image, although 2-dimensional, captures 3-dimensional data - certain filaments are closer than others, and may bend in more ways than just within x-y plane, which is not accurately captured by this formula. This would result in even greater inaccuracy, since all curves are assumed to be within one plane only.

References

Gittes, F., Mickey, B., Nettleton, J., & Howard, J. (1993). Flexural rigidity of microtubules and actin filaments measured from thermal fluctuations in shape. *Journal of Cell Biology*, *120*(4), 923-934. doi.org/10.1083/jcb.120.4.923

Isambert, H., Venier, P., Maggs, A. C., Fattoum, A., Kassab, R., Pantaloni, D., & Carlier, M. F. (1995). Flexibility of actin filaments derived from thermal fluctuations. *Journal of Biological Chemistry*, *270*(19), 11437–11444. https://doi.org/10.1074/jbc.270.19.11437

Niederriter, G., & Martin, D. S. (2019). Length-dependent persistence length for microtubules shorter than 3 micrometers. *Biophysical Journal*, *116*(3), 254a. https://doi.org/10.1016/j.bpj.2018.11.1387

Wisanpitayakorn, P., Mickolajczyk, K. J., Hancock, W., Vidali, O., & Tüzel, E. (2022). Measurement of the persistence length of cytoskeletal filaments using curvature distributions. *Biophysical Journal*, *121*(10), 1813-1822. https://doi.org/10.1016/j.bpj.2022.04.020

a) Native ovalbumin's secondary structure is composed of both alpha-helices and beta-sheets. The cysteine residues, which are located mostly within the interior of the protein, become exposed with denaturation, hence there may be disulfide/sulfhydryl interactions between adjacent denatured ovalbumin molecules (Matsudomi et. al, 1986). An increase in surface hydrophobicity has been observed in denatured ovalbumin, increasing the potential for aggregation through hydrophobic interactions (Kato et. al, 1983). There is an increase in the proportion of beta-sheets compared to alpha-helices, as heat destabilizes hydrogen bonds which stabilize the secondary and tertiary structure (Ngarize et. al, 2004; Hu & Du, 2000). Encouraging protein-protein interaction of heat-denatured molecules has been shown to increase beta-sheet formation, indicating that adjacent ovalbumin molecules are aggregating through cross-linking of beta sheets (Kato & Takagi, 1988).

b) $\Delta G = \Delta H - T\Delta S$

When the egg is boiled, heat is added, which increases T and ΔH. The loss of protein folding results in an increase in disorder, so there is a positive ΔS. At high enough temperatures, $T\,\Delta\,S > \Delta H$ and there is a negative ΔG. This means that the ovalbumin in raw egg has higher free energy than in the hard-boiled egg.

c) Ovalbumin contains a single disulfide bond (Hunginton et. al, 2001). Meanwhile, RNase A contains 4 disulfide bonds, which to stabilize its structure in redox environments, such as the one that Anfinsen used to trigger denaturation (Smardz et. al, 2022). It is also noted that RNase refolds in an "all or nothing" manner, with no partially folded states. One disulfide bond, which triggers changes in the protein's structure locally, cooperates with the formation of the global protein structure. Other proteins may undergo a more gradual process with a greater number of steps and more kinetic traps where the molecule is somewhat stable but not in its native state (Wedemeyer et. al, 2000).

In contrast, ovalbumin is much larger. Since disulfide bonds rely on adjacent sulfhydryl groups, with a larger molecule, it is less likely that they would become close enough for a bond to form randomly. In addition, it becomes trapped in a local free energy minimum due to the formation of protein aggregates. Although it may be more energetically favourable for ovalbumin to return to its native state, gelation results in bonds that have an energetic cost to break.

References

Hu, H. Y., & Du, H. N. (2000). Alpha-to-beta structural transformation of ovalbumin: heat and pH effects. *Journal of Protein Chemistry*, *19*(3), 177-183. https://doi.org/10.1023/a:1007099502179

Kato, A., & Takagi, T. (1988). Formation of intermolecular .beta.-sheet structure during heat denaturation of ovalbumin. *Journal of Agricultural and Food Chemistry*, *36*(6), 1156-1159. https://doi.org/10.1021/jf00084a007

Matsudomi, N., Takahashi, H., & Miyata, T. (2001). Some structural properties of ovalbumin heated at 80°C in the dry state. *Food Research International*, *34*(1-2), 229-235. https://doi.org/10.1016/S0963-9969(00)00157-5

Matsudomi, N., Yamamura, Y., & Kobayashi, K. (1986). Heat-induced aggregation between ovalbumin and lysozyme. *Agricultural and Biological Chemistry*, *50*(6), 1389-1395. https://doi.org/10.1080/00021369.1986.10867601

Ngarize, S., Herman, H., Adams, A., & Howell, N. (2004). Comparison of Changes in the Secondary Structure of Unheated, Heated, and High-Pressure-Treated β-Lactoglobulin and Ovalbumin Proteins Using Fourier Transform Raman Spectroscopy and Self-Deconvolution. *Journal of Agricultural and Food Chemistry*, *52*(21), 6470–6477. https://doi.org/10.1021/jf030649y

Smardz, P., Sieradzan, A. K., & Krupa, P. (2022). Mechanical Stability of Ribonuclease A Heavily Depends on the Redox Environment. *The Journal of Physical Chemistry. B*, *126*(33), 6240–6249. http://doi.org/10.1021/acs.jpcb.2c04718

Wedemeyer, W. J., Welker, E., Narayan, M., & Scheraga, H. A. (2000). Disulfide Bonds and Protein Folding. *Biochemistry*, *39*(15), 4207-4216. https://doi.org/10.1021/bi992922o